Supporting Information

Synthesis and Photocatalytic Activity of Porous Bismuth Oxychloride Hexagonal Prisms

Liyong Ding,[a] Huan Chen,[a] Qingqian Wang,[a] Tengfei Zhou,[b] Qingqing Jiang,[a] Yuhong Yuan,[a] Jinlin Li [a] and Juncheng Hu[a]*

a Key Laboratory of Catalysis and Materials Science of the State Ethnic Affairs Commission & Ministry of Education, South-Central University for Nationalities, Wuhan, 430074, PR China
*Tel: +86 27 67841302; E-mail: jchu@mail.scuec.edu.cn
b Institute for Superconducting and Electronic Materials, School of Mechanical, Materials and Mechatronics Engineering, University of Wollongong, North Wollongong, New South Wales 2500, Australia

1 Experimental section

1.1 Preparation of porous BiOCl HPs

All of the chemicals were purchased from Sinopharm Chemical Reagent Co., Ltd. (Shanghai, China), analytical grade, and used as received without any further treatment. In our synthesis procedure, 2.426 g bismuth nitrate ($Bi(NO_3)_3 \cdot 5H_2O$) was first dissolved in 15 mL acetic acid (CH_3COOH). After complete dissolution, 60 mL methanol (CH_3OH) was added under vigorous stirring. Subsequently, 0.7548 g glucosamine hydrochloride ($C_6H_{13}NO_5 \cdot HCl$) were dispersed into above solution. Then the mixture was transferred into an autoclave a 100 mL Teflon-lined stain-less steel autoclave, followed by heating and maintaining at 180 °C for 5 h, and then naturally cooled to ambient temperature. The resulting precipitates were washed with deionized water and ethanol thoroughly to remove residual ions and dried at 60 °C overnight.

1.2 Characterization

XRD patterns were collected on a Bruker D8 Advance X-ray diffractometer operated at 40 kV and 40 mA with Ni filtered Cu Kα radiation (λ= 1.5404 Å). SEM images and EDX elemental mapping were observed with SU8010 (Hitachi, Japan). TEM observation and the EDX spectrum were carried out with Tecnai G2 F30 (FEI, Holland). X-ray photoelectron spectroscopy (XPS) measurements were conducted on a VG Multilab 2000 (VG Inc.). The Brunauer-Emmett-Teller (BET) specific surface areas of the samples were evaluated on the basis of nitrogen adsorption isotherms using a Micromeritics ASAP 2020 gas adsorption apparatus (USA). The fourier transform infrared (FTIR) spectra were recorded on a Nexus470 FTIR ESR (Nicolet, USA) using KBr as background. UV-vis diffused spectrum (DRS) was measured using the diffuse reflectance method with a Shimadzu UV-

2550 spectrophotometer using an integrating sphere accessory. $BaSO_4$ was used as a reference materials in UV-vis diffuse experiments.

1.3 Evaluation of photocatalytic activity

The photocatalytic activity of the samples was evaluated by the degradation of methyl orange (MO) (50 mL, 10 $mg \cdot L^{-1}$) under visible light and ultraviolet light irradiation, respectively, using a 350 W Xe lamp with a 420 nm and 365 nm cutoff filter. In each experiment, 50 mg of catalysts was suspended in aqueous solution. The suspensions were magnetically stirred in the dark for 1 h to ensure the establishment of an adsorption/desorption equilibrium between the organics and the catalyst, then the suspensions were vertically irradiated. At given irradiation time intervals, 3 mL solution was sampled, centrifuged, and then filtered through a Millipore filter (pore size 0.45 μm) to remove the catalyst particulates. The concentration of MO was analyzed by the UV-Vis spectrometer measurement (UV-2550, Shimadzu).

The photocatalytic selective oxidation of benzyl alcohol under visible light and simulated sunlight conditions. A mixture of benzyl alcohol (5 μL) and 50 mg of catalyst was dissolved in the solvent of toluene (50 mL), 33 mg K_2CO_3 was added and then feeding oxygen constantly. Subsequently, the mixture was transferred into a 100 mL Pyrex glass bottle. The suspension was vigorous stirred and irradiated by a 350 W Xe lamp with a 420 nm cutoff filter or not. After the reaction, the mixture was centrifuged to completely remove the catalyst particles. The remaining solution was analyzed with an FULI Gas Chromatograph (GC9790Ⅱ).

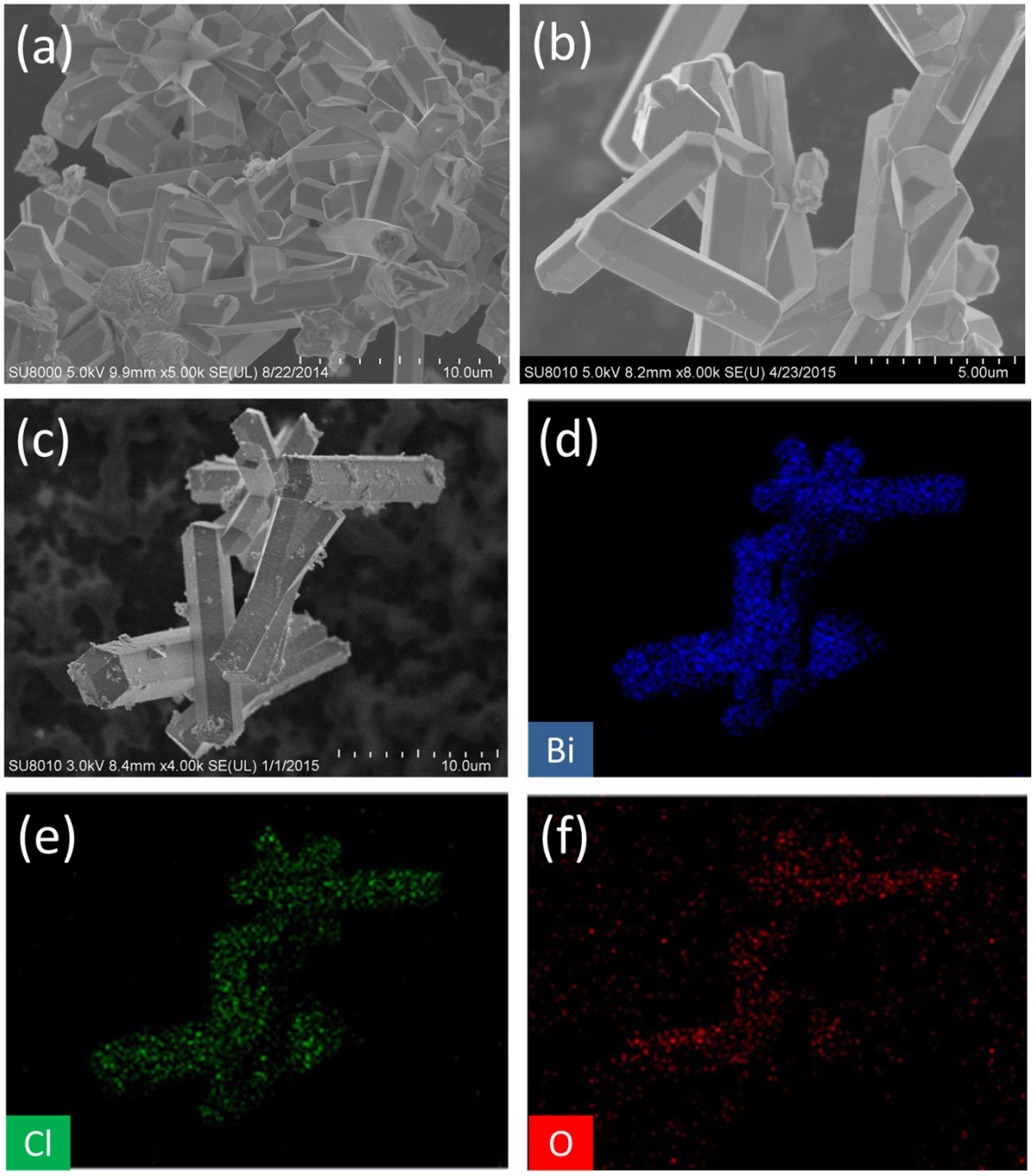

Fig. S1 (a,b)The FESEM images of porous BiOCl HPs. (c-f) EDX elemental mapping.

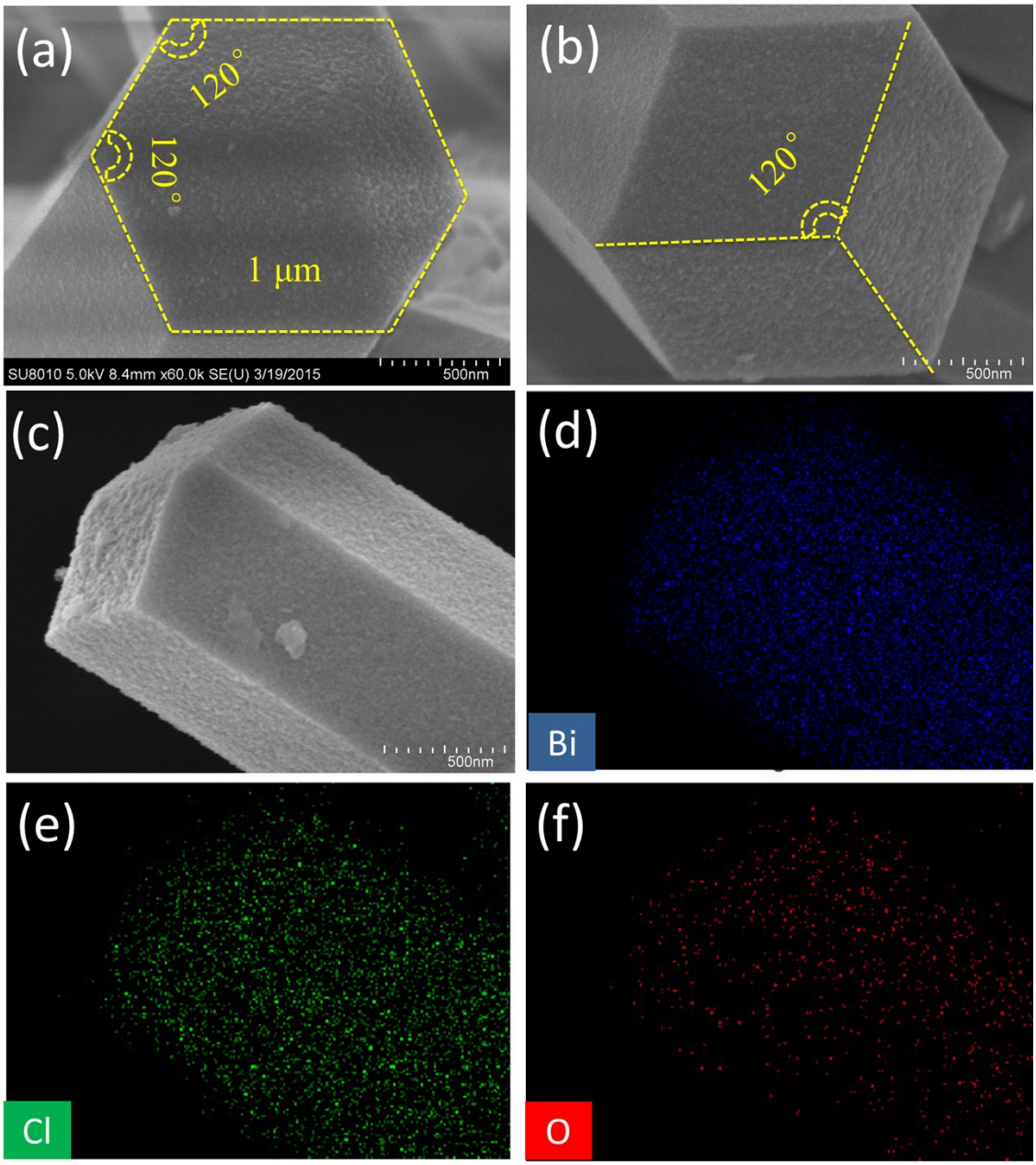

Fig. S2 (a,b) HRSEM of a single porous BiOCl HPs. (c-f) The EDX elemental mapping of a single porous BiOCl HPs.

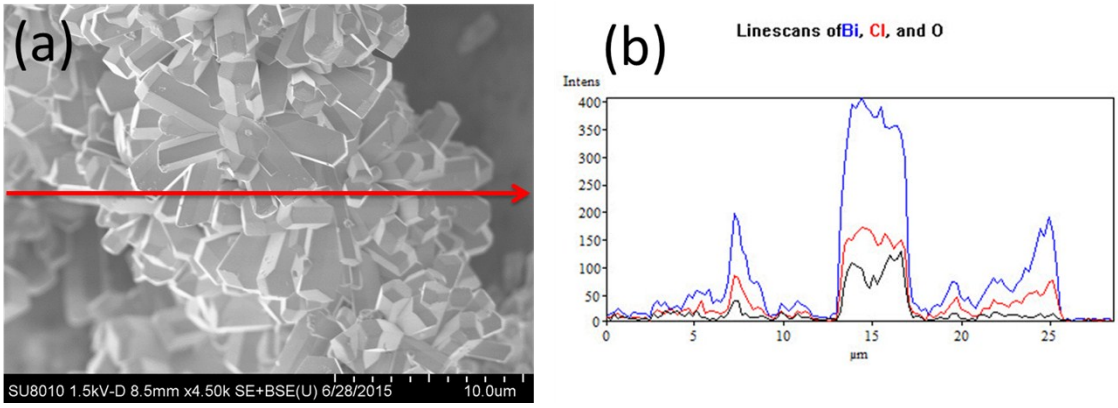

Fig. S3 The SEM-EDX linescans of porous BiOCl HPs.

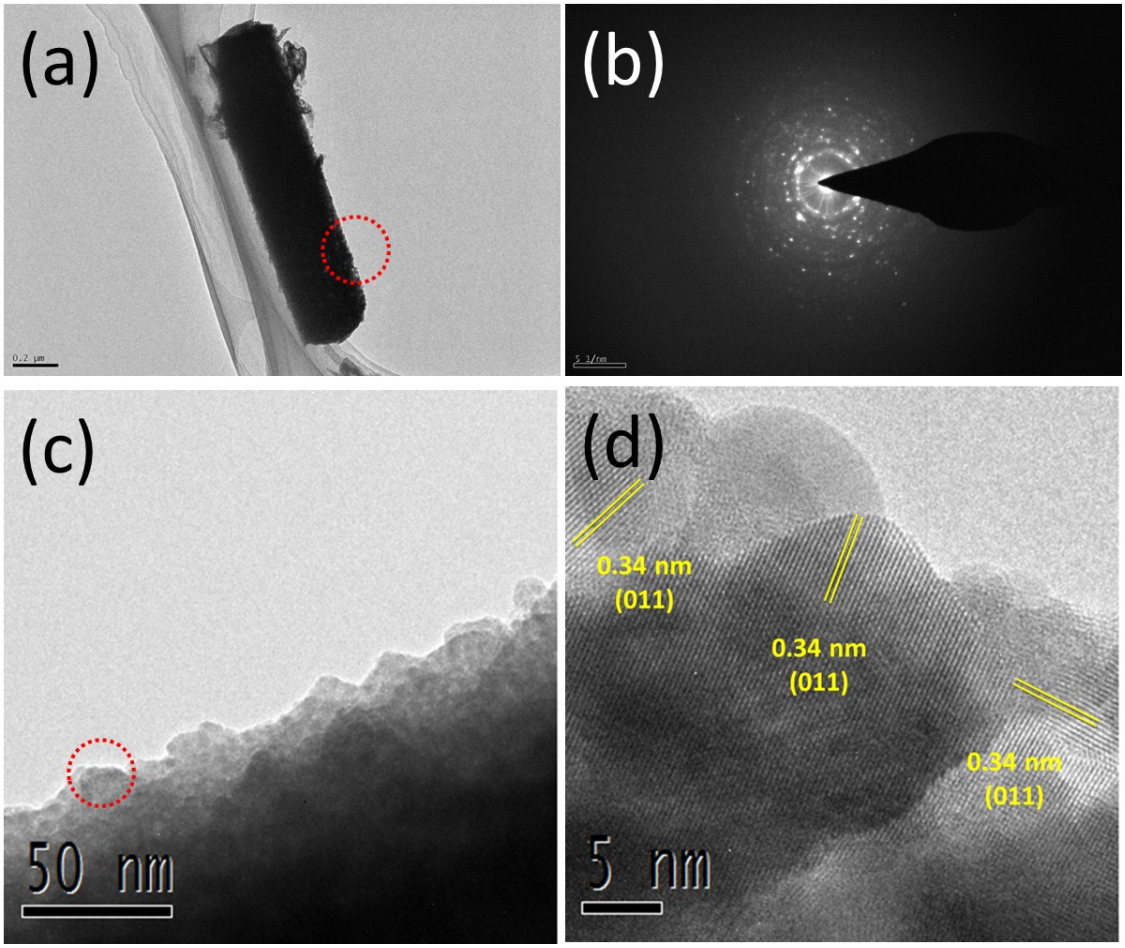

Fig. S4 (a) TEM image with low magnification. (b) The selected area electron diffraction (SAED) pattern. (c) TEM image with high magnification. (d) HRTEM image.

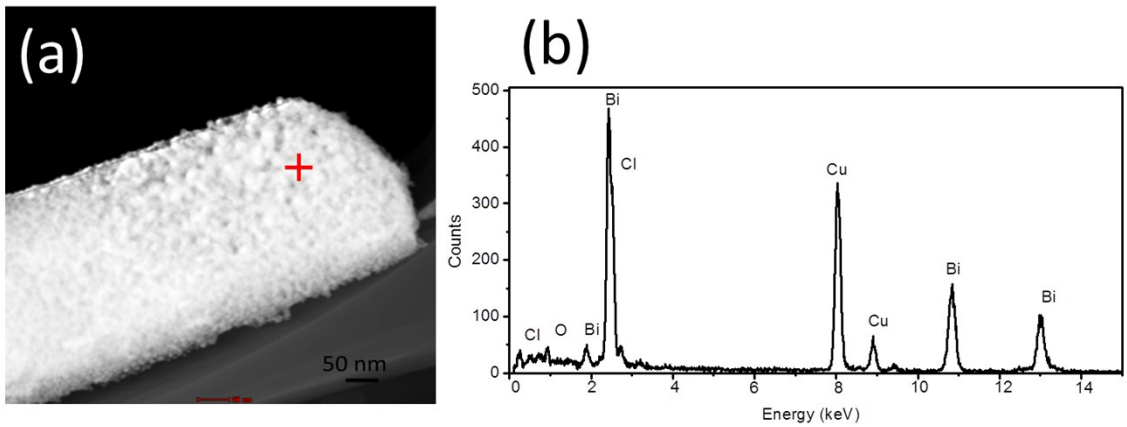

Fig. S5 The high-angle annular dark-field (HAADF)-scanning STEM-EDX dot scan of porous BiOCl HPs.

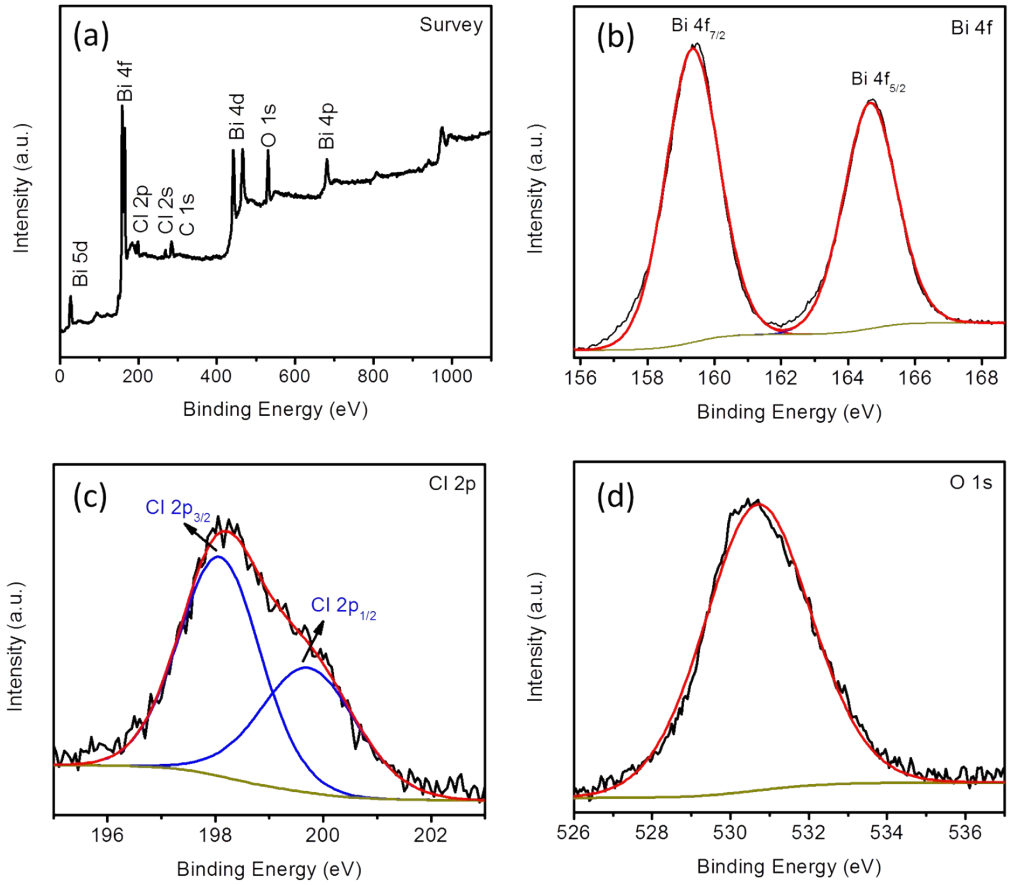

Fig. S6 XPS spectra: (a) survey spectrum, (b) Bi 4f, (c) Cl 2p, (d) O 1s of porous BiOCl HPs.

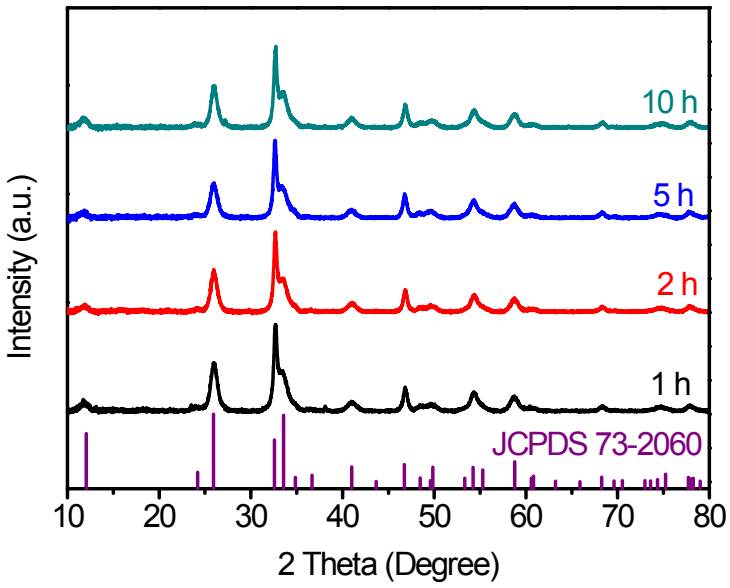

Fig. S7 XRD patterns of porous BiOCl HPs at different reaction times.

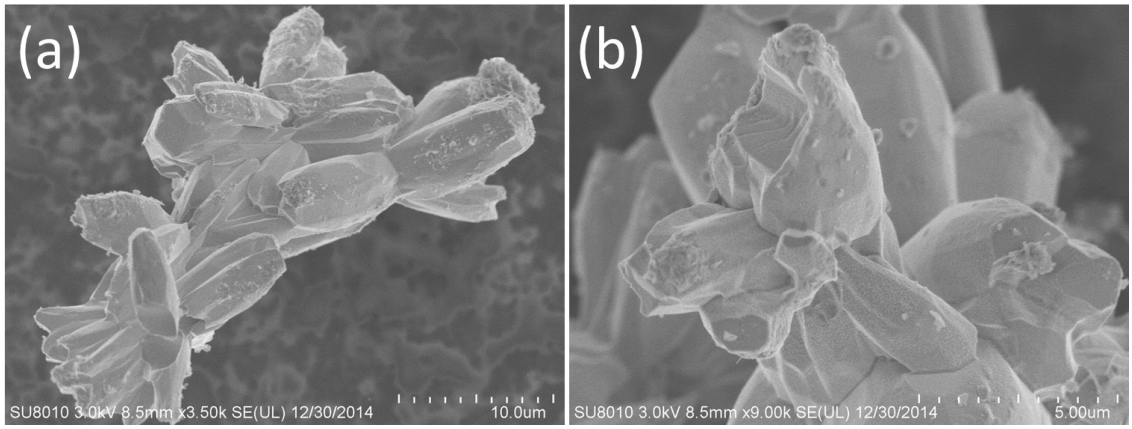

Fig. S8 FESEM images of BiOCl HPs obtained at 180 °C, 1 h.

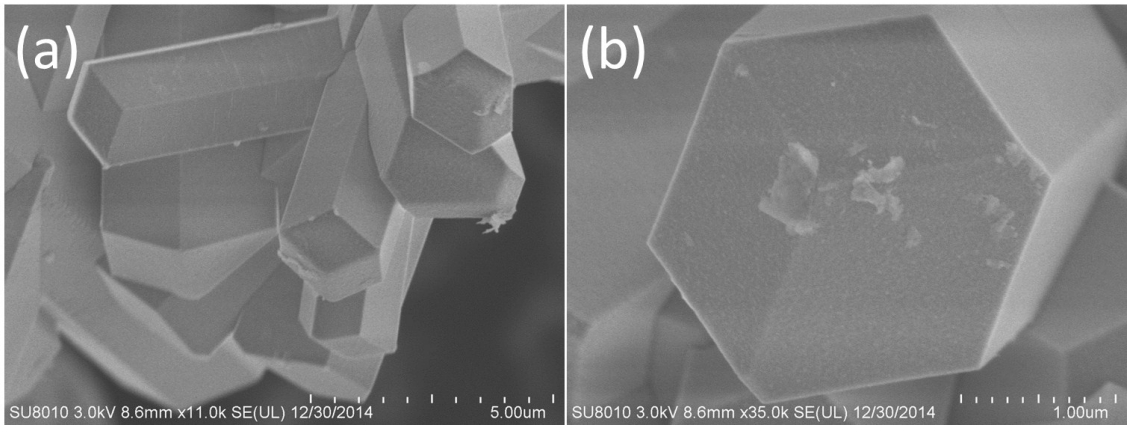

Fig. S9 FESEM images of BiOCl HPs obtained at 180 °C, 2 h.

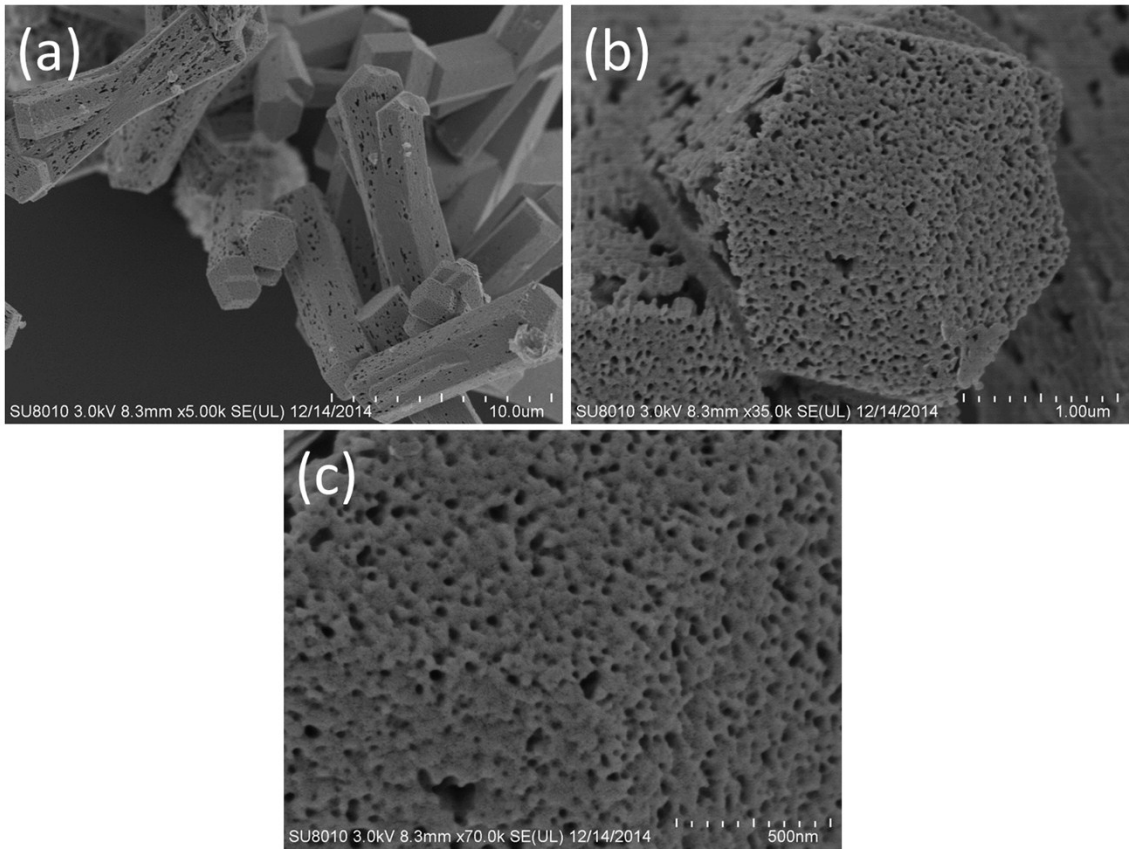

Fig. S10 FESEM images of BiOCl HPs obtained at 180 °C, 5 h.

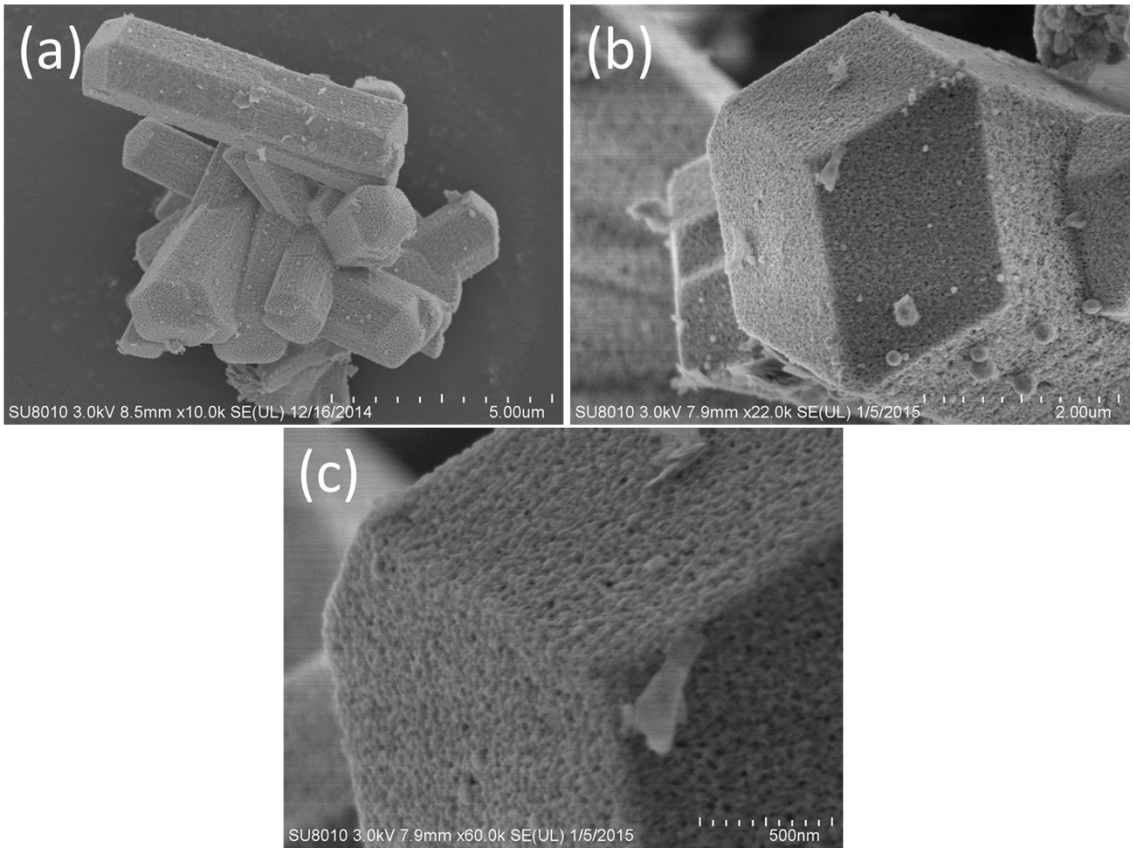

Fig. S11 FESEM images of BiOCl HPs obtained at 180 °C, 10h.

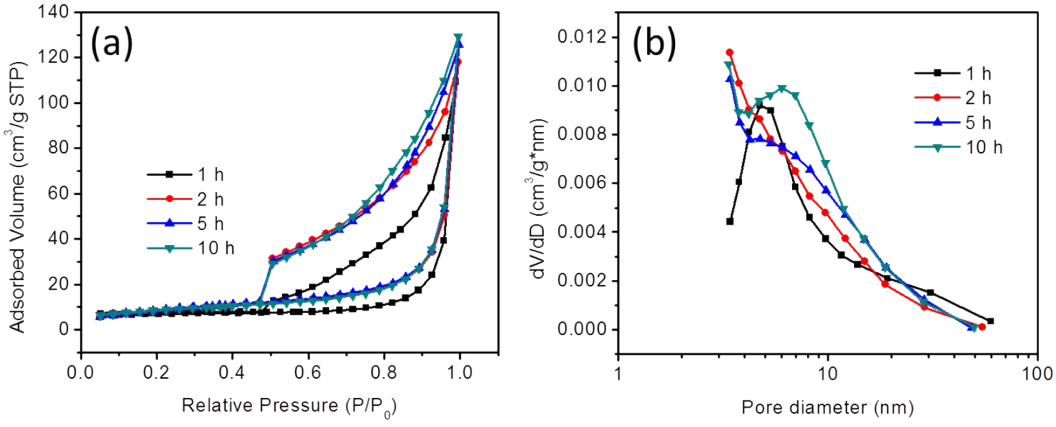

Fig. S12 (a) N_2 adsorption-desorption isotherms. (b) pore size distributions.

Table S1. BET surface area and pore volume of porous BiOCl HPs at different reaction time.

	1 h	2 h	5 h	10 h
S_{BET} (m^2/g)	23.7	30.5	32.1	30.2
V_{BJH} (cm^3/g)	0.17	0.18	0.19	0.20

A nitrogen adsorption-desorption isotherms are measured to determine the specific surface area and pore size of the samples. These shapes of all the isotherms with hysteresis loop correspond to type Ⅳ isotherm according to the Brunauer-Deming-Teller (BDDT) classification, indicating the presence of mesopores in these samples, which are formed through the aggregation of the nanoparticles. More specifically, the porous BiOCl HPs at 5 h possess the larger adsorption volume and specific surface area of 32.1 m^2/g. It is greatly match with the FESEM images of BiOCl reacted for different reaction times.

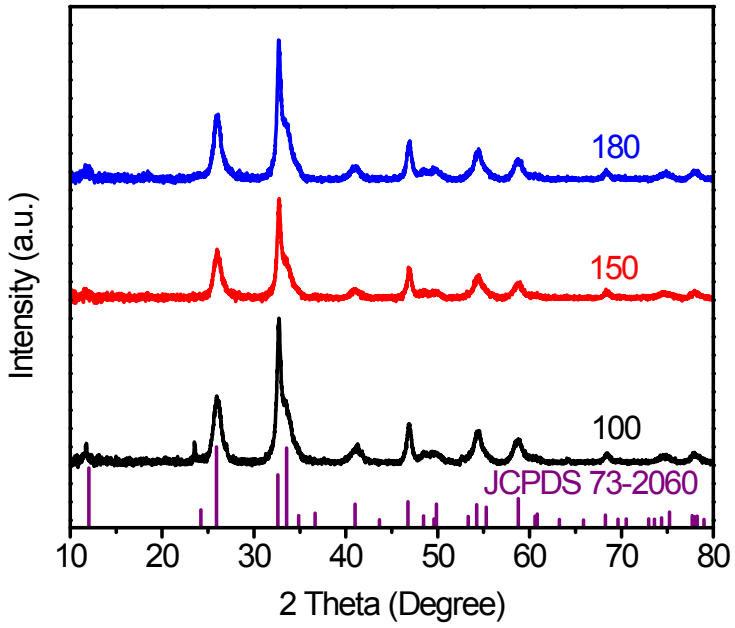

Fig. S13 XRD patterns of porous BiOCl HPs at different temperatures.

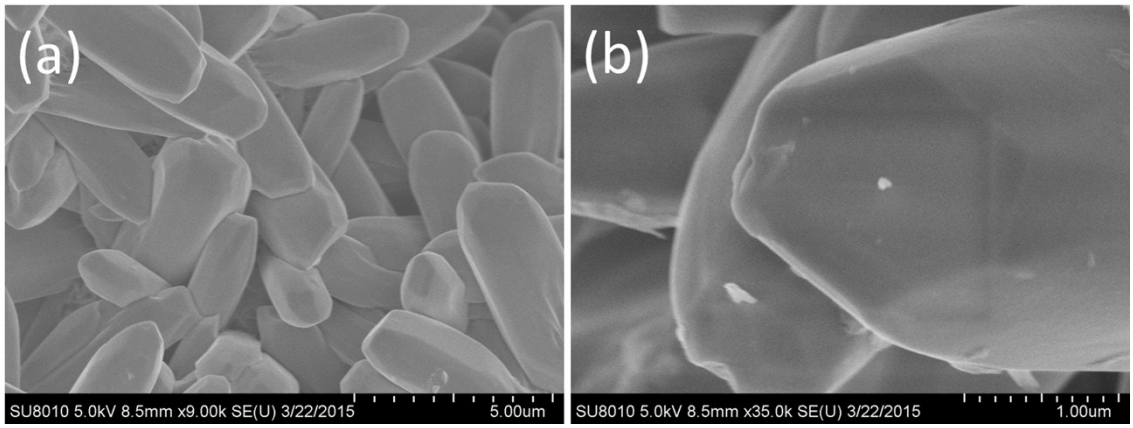

Fig. S14 FESEM images of BiOCl HPs obtained at 100 °C, 5 h.

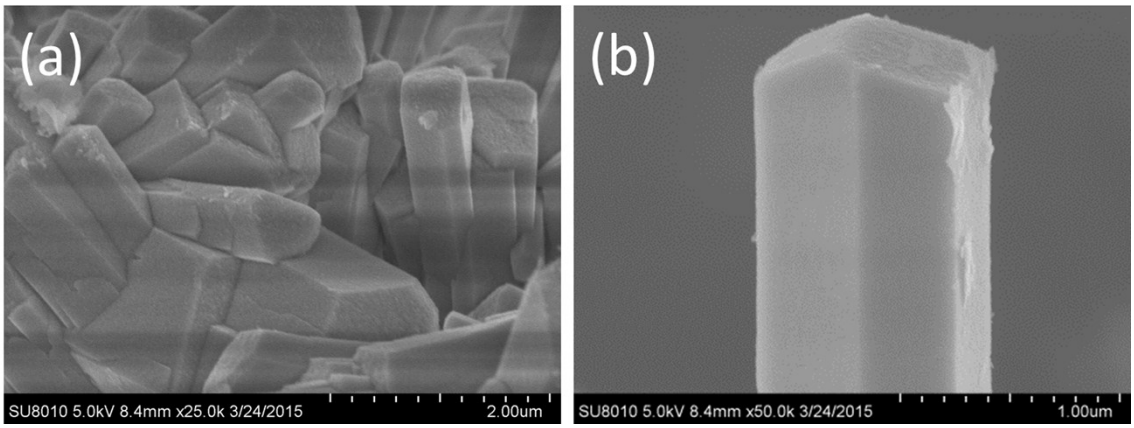

Fig. S15 FESEM images of BiOCl HPs obtained at 150 °C, 5 h.

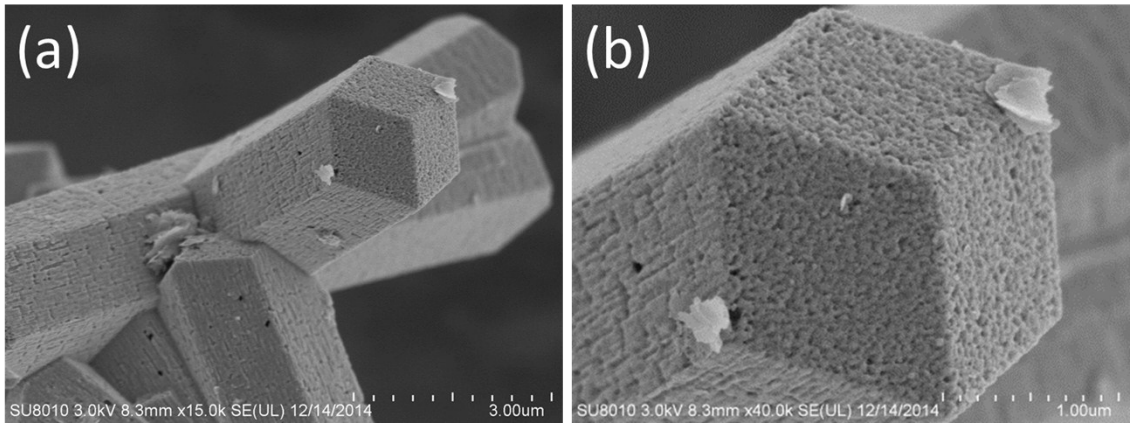

Fig. S16 FESEM images of BiOCl HPs obtained at 180 °C, 5 h.

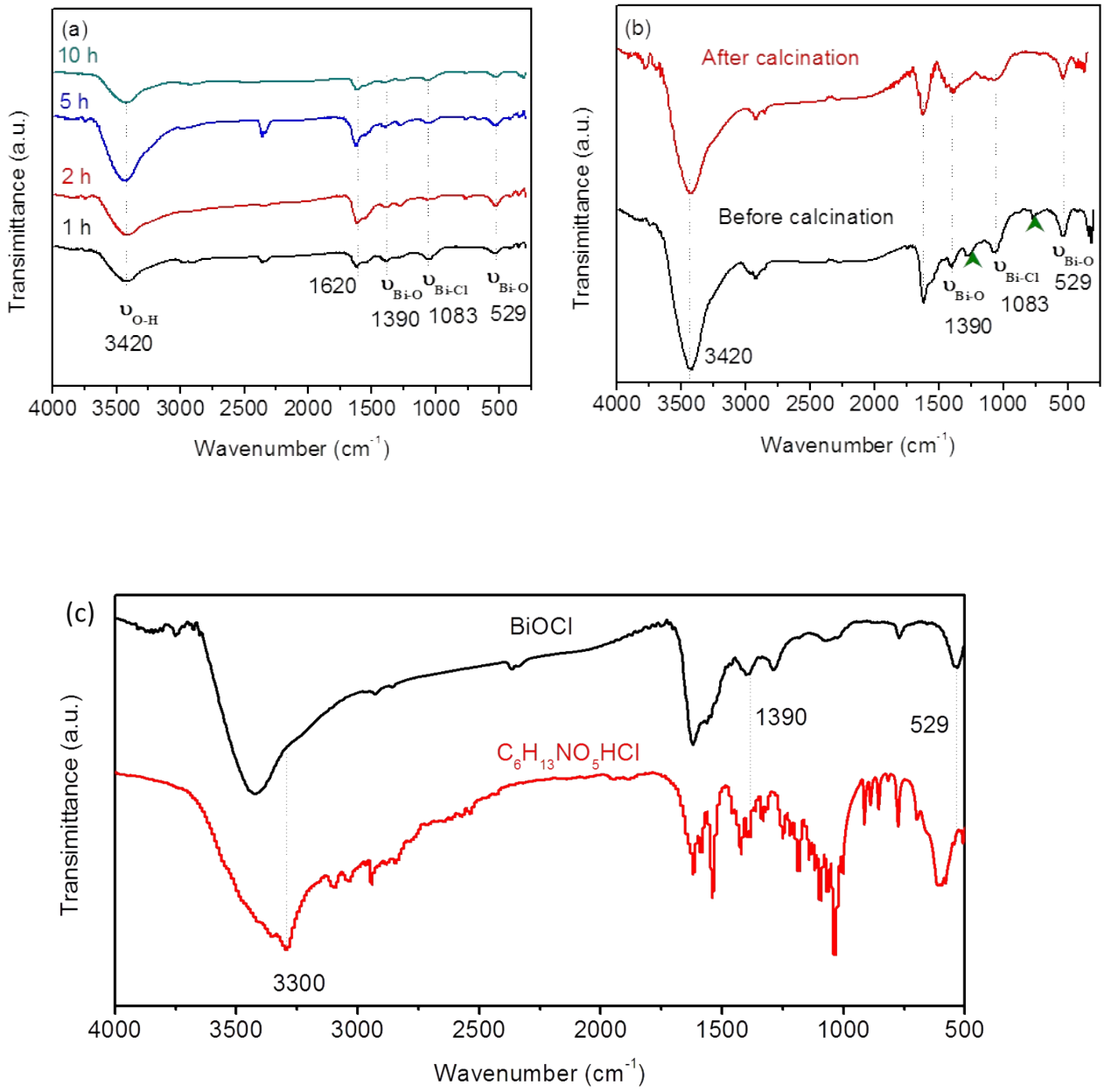

Fig. S17 FTIR spectra: (a) BiOCl HPs obtained at different reaction times, (b) BiOCl HPs before and after calcination, (c) BiOCl HPs and glucosamine hydrochloride.

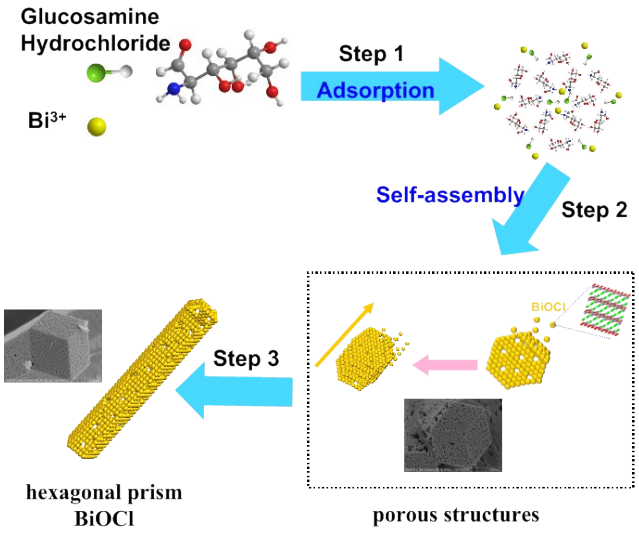

Fig. S18 Schematic illustration of the possible formation mechanism of porous BiOCl HPs.

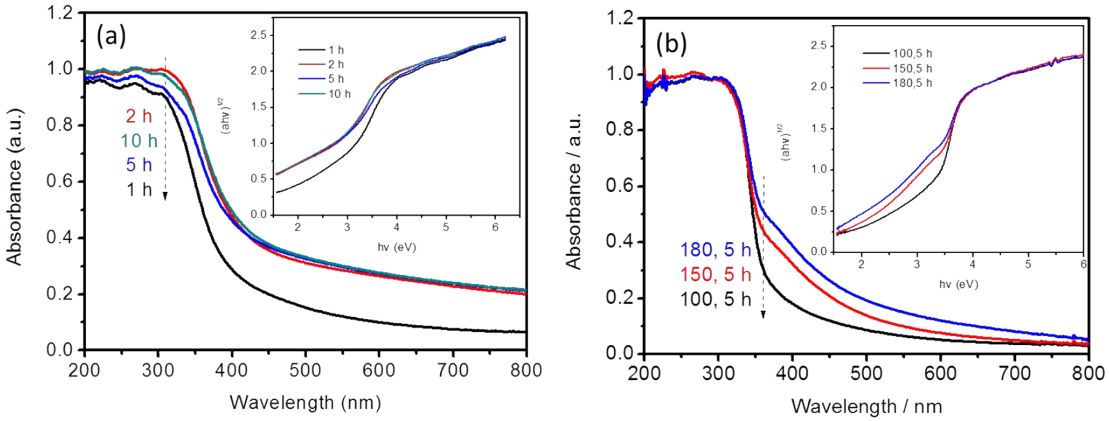

Fig. S19 UV-vis diffuse reflectance spectra and plots of $(\alpha h\upsilon)^{1/2}$ versus photon energy ($h\upsilon$) of BiOCl samples (inset) prepared at different reaction times (a) and temperatures (b).

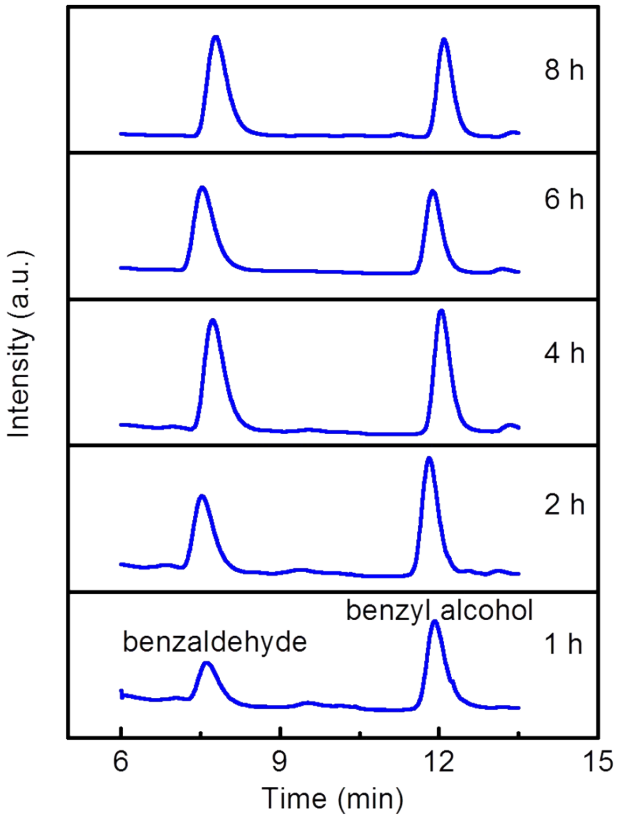

Fig. S20 GC patterns of the photocatalytic oxidation of benzyl alcohol over the sample obtained at 5 h.

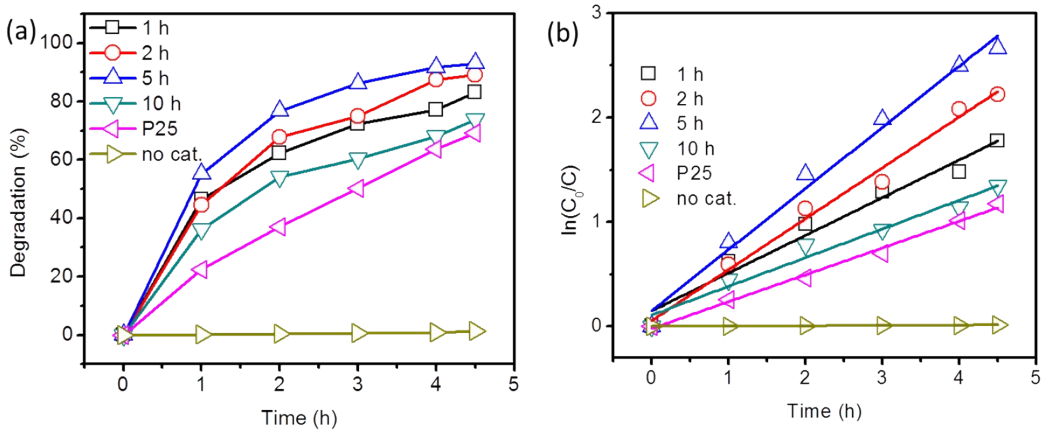

Fig. S21 (a) Comparative studies of MO degradation under visible light irradiation over as-prepared samples. (b) Kinetic fit for the degradation of MO with different catalysts under visible light irradiation.

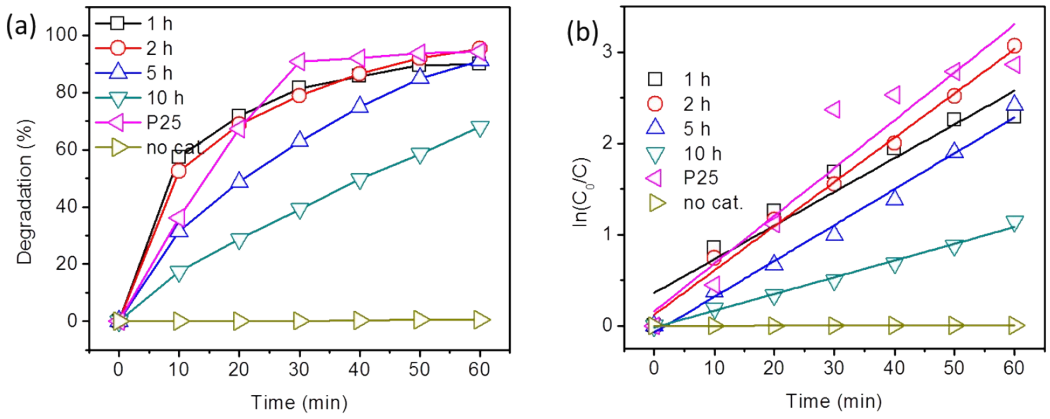

Fig. S22 (a) Comparative studies of MO degradation under UV light irradiation over as-prepared samples. (b) Kinetic fit for the degradation of MO with different catalysts under UV light irradiation.

Table S2. The apparent reaction rate constants for photocatalytic degradation of MO under visible light and UV light.

k	1 h	2 h	5 h	10 h	P25	no cat.
Vis (h^{-1})	0.36136	0.48791	0.58562	0.27499	0.25726	0.00281
UV (min^{-1})	0.03697	0.04858	0.03937	0.01838	0.05244	$9.2464E^{-5}$

The photocatalytic degradation of MO is a pseudo-first-order reaction and its kinetics can be described as follows: $\ln(C_0/C)=kt$. Where k is the apparent reaction rate constant, and t is their radiation time, C_0 and C are the concentrations of MO aqueous solution at irradiation times of 0 and t, respectively. The calculated apparent reaction rate constants k of the different samples are listed in Table S2.

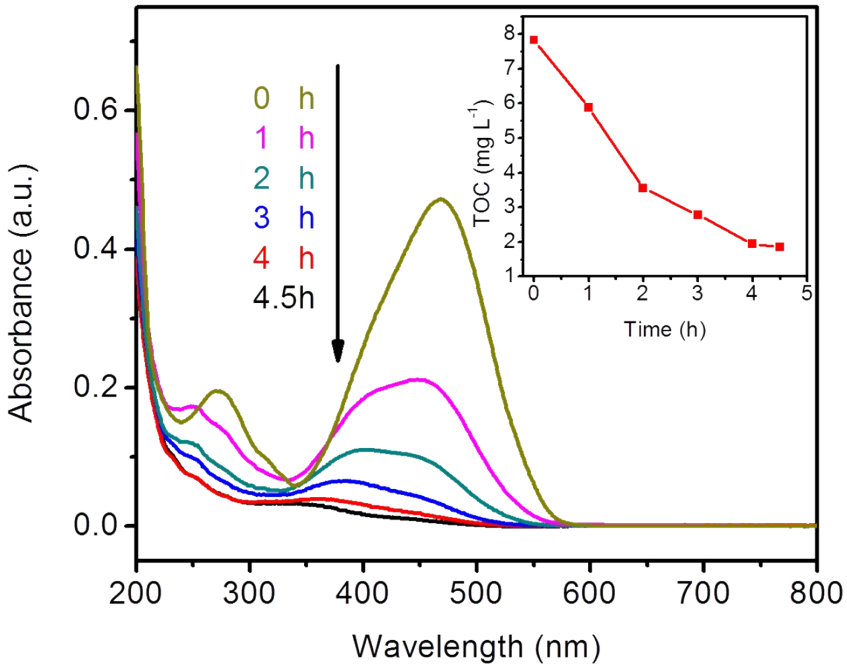

Fig. S23 The temporal evolution of the absorption spectra of MO in the presence of the BiOCl HPs, the inset is the change of corresponding TOC values of MO at different time.

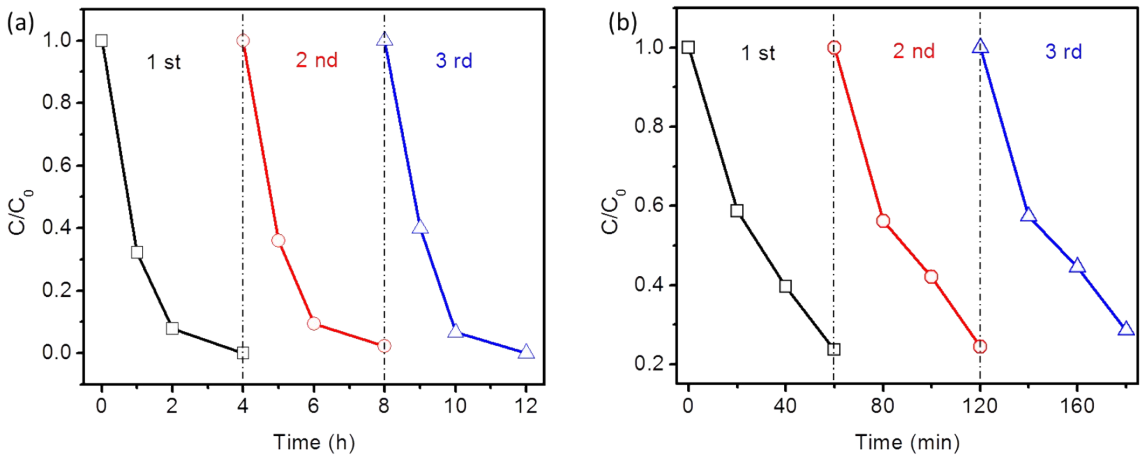

Fig. S24 Photocatalytic degradation of MO by BiOCl HPs in repeated experiments under (a) visible light and (b) UV light irradiation.

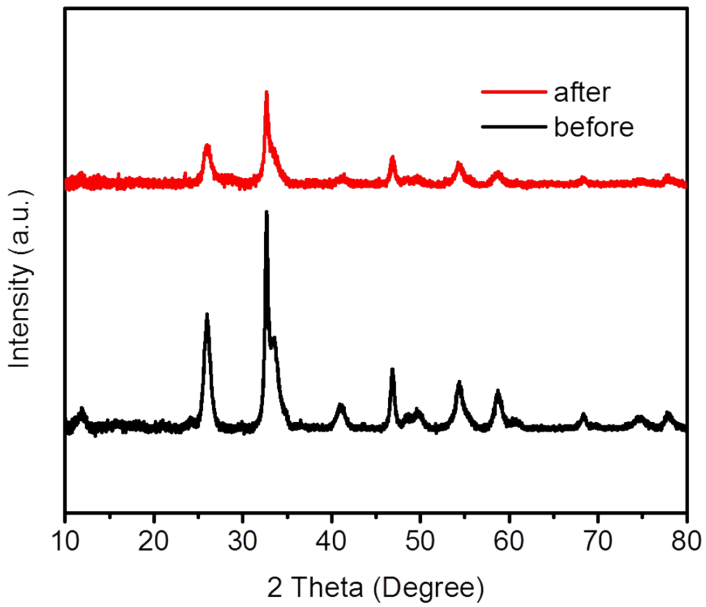

Fig. S25XRD patterns of the BiOCl HPs before and after photocatalytic reaction.

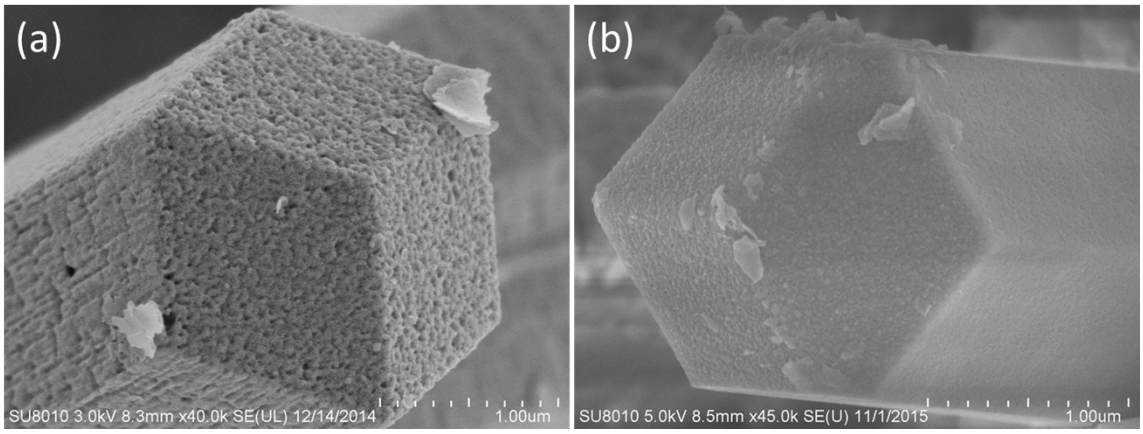

Fig. S26SEM images of BiOCl HPs (a) before and (b) after photocatalytic reaction.